doi:10.1093/plphys/kiab217 PLANT PHYSIOLOGY 2021: 187: 2246–2261

Plant Physiology®

Research Article

Nutrient cycling is an important mechanism for homeostasis in plant cells

Ingo Dreyer [1,*,†]

1 Center of Bioinformatics, Simulation and Modeling (CBSM), Faculty of Engineering, Universidad de Talca, Talca CL-3460000, Chile

*Author for communication: idreyer@utalca.cl
†Senior author.

I.D. conceived the project, designed the experiments, analyzed the data, prepared the figures, and wrote the article.

The author responsible for distribution of materials integral to the findings presented in this article in accordance with the policy described in the Instructions for Authors (https://academic.oup.com/plphys/pages/general-instructions) is: Ingo Dreyer (idreyer@utalca.cl).

Abstract

Homeostasis in living cells refers to the steady state of internal, physical, and chemical conditions. It is sustained by self-regulation of the dynamic cellular system. To gain insight into the homeostatic mechanisms that maintain cytosolic nutrient concentrations in plant cells within a homeostatic range, we performed computational cell biology experiments. We mathematically modeled membrane transporter systems and simulated their dynamics. Detailed analyses of 'what-if' scenarios demonstrated that a single transporter type for a nutrient, irrespective of whether it is a channel or a cotransporter, is not sufficient to calibrate a desired cytosolic concentration. A cell cannot flexibly react to different external conditions. Rather, at least two different transporter types for the same nutrient, which are energized differently, are required. The gain of flexibility in adjusting a cytosolic concentration was accompanied by the establishment of energy-consuming cycles at the membrane, suggesting that these putatively "futile" cycles are not as futile as they appear. Accounting for the complex interplay of transporter networks at the cellular level may help design strategies for increasing nutrient use efficiency of crop plants.

Introduction

For plants as for animals, control of (ion) homeostasis is crucial to establish defined conditions within cells and cellular compartments that allow various biochemical processes to take place in a controlled manner. Homeostatic processes are therefore fundamental for plant life development and resilience to even hostile environments. A critical role in (ion) homeostasis is played by membrane transport proteins. As estimated for Arabidopsis (*Arabidopsis thaliana*), around 18% of the predicted proteins of a plant genome may contain two or more transmembrane domains, and approximately over half of those may perform transporter functions (Ward, 2001; Schwacke et al., 2003; Tang et al., 2020). Although our knowledge on the function, the tissue-specific expression and subcellular localization of plant membrane transporters increases daily, detailed mechanistic insights into the functional interplay between these transporter proteins are still largely missing. This gap in knowledge might be a severe obstacle in developing strategies and approaches involving transporter proteins to improve nutrient use efficiency and tolerance to environmental stresses, as well as to boost general crop fitness and productivity.

The analysis of membrane transporter networks is not a trivial task, and is almost impossible to accomplish with exclusively wet-laboratory approaches. Nevertheless, transporter types can be mathematically described, allowing deep insights into the dynamics of transporter networks via computational analyses (Dreyer and Michard, 2020).

Received April 1, 2021. Accepted April 23, 2021. Advance access publication May 7, 2021

Computational modeling already helped to better understand guard cell movement (Hills et al., 2012; Blatt et al., 2014), the role of K^+ gradients in energizing phloem (re)loading processes (Gajdanowicz et al., 2011; Dreyer et al., 2017), the nutrient exchange in mycorrhizal symbioses (Schott et al., 2016; Dreyer et al., 2019; Nizam et al., 2019), the mechanism and potential consequences of vacuolar excitability (Jaślan et al., 2019; Dindas et al., 2021), and touch-sensitive signaling in trigger hairs of the Venus flytrap (Iosip et al., 2020).

The present study was inspired by the efforts to optimize K^+ use efficiency in crop plants (Zörb et al., 2014). A large variety of K^+ transporters that are employed by plants for the task of K^+ uptake and redistribution has been identified. In addition, our knowledge on the signaling cascades that regulate the activity of these transporters is growing daily (for reviews, see, e.g. Dreyer and Uozumi, 2011; Sharma et al., 2013; Ahmad and Maathuis, 2014; Anschütz et al., 2014; Chérel et al., 2014; Nieves-Cordones et al., 2014; Shabala and Pottosin, 2014; Véry et al., 2014; Luan et al., 2017; Sze and Chanroj, 2018; Chérel and Gaillard, 2019; Ragel et al., 2019). Nevertheless, it is still not clear which constraints set limits to a cell to control the cytosolic K^+ concentration by adjusting transporter activities in response to external conditions. To address this knowledge gap, in this study computational cell biology experiments have been designed that provide comprehensible insight into a cell's ability to control cytosolic $[K^+]$ under given external conditions. The topic is approached in thought experiments ('what-if' scenarios) to illustrate the straightforward conclusions from basic thermodynamics of membrane transport and mathematical considerations. This approach allowed understanding of general fundamental principles of homeostasis that permit a living compartment (a cell or an organelle) to set defined internal conditions. Although the motivating starting point was K^+ nutrition, the results could be generalized to other nutrients. The conclusions presented here provide fundamental insights into the interplay between different transporters and expose essential features needed to control homeostasis. These insights might provide important theoretical knowledge for future attempts to optimize nutrient use efficiency in crop plants.

Results

The goal of this study was to answer the question, how much can a plant cell adjust the steady state of internal concentrations and the membrane voltage by changing membrane transporter activities. This is not a trivial problem and can easily reach a complexity that goes beyond our imagination. To gain insights nevertheless, a step-wise synthetic computational cell biology approach was chosen. Starting from the analysis of the simplest systems, the complexity was successively increased in order to learn how this affects the flexibility of the systems. In a first set of thought experiments, a cell that is surrounded only by the plasma membrane was considered. That is, at that stage the effects introduced by organelles like the vacuole were eliminated. This type of complexity was added in a subsequent step. The conceptional approach is presented first for the case of the most abundant cation in plants, K^+, followed by countercharge-providing anions, and finally for sugar as an example of an uncharged nutrient and of metabolic processes. In all the models, the proton concentrations were kept constant because they are predominantly determined by metabolic processes and, particularly in the steady state, not by transporter processes (Sanders and Slayman, 1982; Wegner and Shabala, 2020; Wegner et al., 2021).

The control of $[K^+]_{cyt}$ implies the control of E_K

An important note at the beginning, membrane transport processes are ruled by the transmembrane (electro)chemical gradient of the nutrient in question. This gradient does not depend solely on the cytosolic concentration (e.g. $[K^+]_{cyt}$), but on the logarithm of the ratio of the concentrations on both sides of the membrane ($E_K = \frac{RT}{F} \cdot \ln\left(\frac{[K]_{apo}}{[K]_{cyt}}\right)$, in the case of potassium with gas constant R, absolute temperature T, and Faraday constant F). This has fundamental mechanistic consequences for a cell's ability to control cytosolic concentrations. By adjusting the activities of the membrane transporters, a cell cannot control $[K^+]_{cyt}$ directly, but primarily only E_K. By flexibly adapting E_K according to the external conditions, $[K^+]_{cyt}$ can in turn be controlled and maintained constant. In other words, in order to respond to a wider range of external conditions when holding $[K^+]_{cyt}$ constant, a cell must be able to adjust E_K over a wider range. The same holds true for other ions and metabolites.

Case 1: Only K^+ channels

A first 'what-if' scenario considered a case in which the proton H^+-ATPase acted together with K^+ channels. In such a system, the H^+-ATPase pumped H^+ out of the cell, while the open potassium channel allowed the influx of K^+ that electrically compensated for the H^+ efflux (Figure 1, A and B). The accumulation of K^+ in the cell led to a negative shift of E_K, which also negatively shifted the voltage at which the H^+ efflux compensated the K^+ influx. A stable steady state could only be reached in this system if $I_P(V) = 0$ and $E_K = V$. This means that the membrane voltage adjusted to the steady-state voltage of the H^+-ATPase, and also that E_K was fixed to this value. There was neither a net K^+ flux via the channel nor a net H^+ flux via the pump under this condition. To get an idea about which K^+ gradients could be established with such a system, a pH gradient of $pH_{cyt} = 7.0/pH_{apo} = 6.0$ and a steady-state voltage of $V_{0,pump} = -200$ mV were considered. For an external K^+ concentration of $[K^+]_{apo} = 100$ µM, the internal concentration would have equilibrated at $[K^+]_{cyt} = 300$ mM, and for $[K^+]_{apo} = 1$ mM the steady state was at $[K^+]_{cyt} = 3$ M. These cation concentrations would need to be charge-balanced by anions,

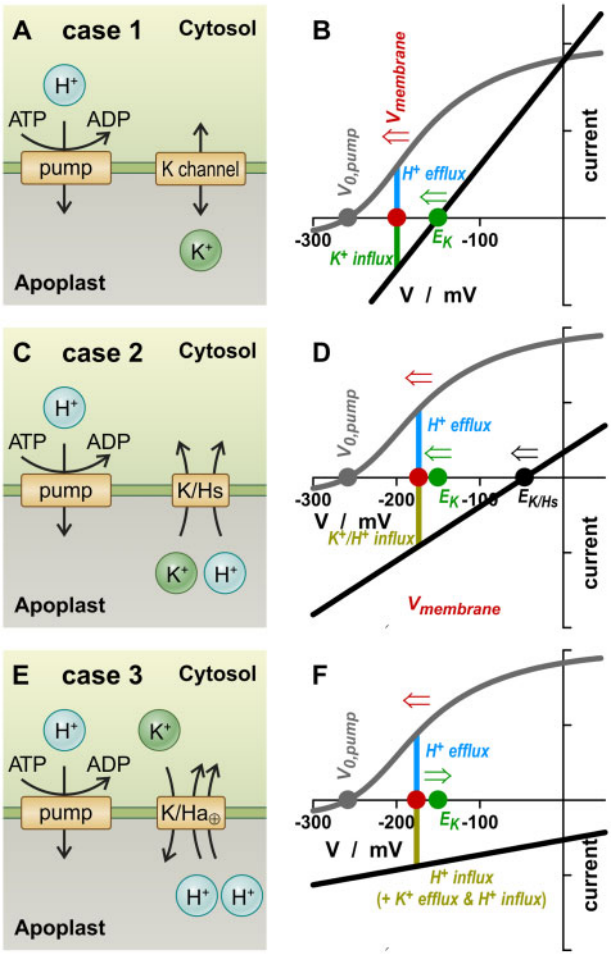

Figure 1 E_K and V as adjusted by single K^+ transporters and the H^+ pump. A and B, Case 1, only K^+ channels. The H^+ efflux (blue line) is electrically compensated by a K^+ influx (green line). The K^+ influx shifts E_K (green dot) and consequently also $V_{membrane}$ (red dot) to more negative voltages. The only stable steady state of the system is $E_K = V_{0,pump}$ (grey dot). C and D, Case 2, only K^+/H^+ symporters. The H^+ efflux (blue line) is electrically compensated by the K^+/H^+ influx (ochre line). The K^+ influx shifts E_K (green dot), $E_{K/Hs}$ (black dot) and consequently also $V_{membrane}$ (red dot) to more negative voltages. The only stable steady state of the system is $0.5 \cdot (E_K + E_H) = V_{0,pump}$ (grey dot), that is, $E_K = 2 \cdot V_{0,pump} - E_H$. E and F, Case 3, only K^+/H^+ antiporters. In case of electrogenic $K^+/2H^+$ antiporters, the pump-mediated H^+ efflux (blue line) is electrically compensated by the H^+-mediated charge surplus of the antiport (ochre line). The K^+ efflux shifts E_K (green dot) to more positive voltages and $V_{membrane}$ (*red dot*) to more negative voltages. In general, the steady state of this system is $(n-1)^{-1} \cdot (n \cdot E_H - E_K) = V_{0,pump}$ (grey dot), that is, $E_K = n \cdot E_H - (n-1) \cdot V_{0,pump}$.

for instance malate^{2-}, originating from metabolic processes that also provide the protons pumped out of the cell. The consequences of anion transport and metabolic processes are considered further below. The steady state of case 1 was determined exclusively by the voltage at which the pump current was zero (parameter $V_{0,pump}$ in Eq. 1). This parameter depends on the energetic status of the cell and the transmembrane pH gradient. If, besides for the pump and K^+ channel, there were other transporters in the membrane that were not involved in K^+ transport, they would consume part of the energy provided by the H^+-ATPase. As will be shown later in this article, such a situation can be simulated in the considered steady-state model simply by adjusting the parameter $V_{0,pump}$. With $V_{0,pump} = -125$ mV, the results were qualitatively identical as with $V_{0,pump} = -200$ mV. However, E_K would now be -125 mV in the steady state and the K^+ gradients $[K^+]_{apo} = 100\ \mu M/[K^+]_{cyt} = 14.8$ mM and $[K^+]_{apo} = 1$ mM/$[K^+]_{cyt} = 148$ mM. Thus, the cell can control E_K and $[K^+]_{cyt}$ indirectly via the energy not dissipated elsewhere, and therefore available for K^+ transport. However, a direct control of V or E_K by varying the K^+ channel activity was not possible.

Case 2: Only K^+/H^+ symporters

A second 'what-if' scenario considered a case in which the proton H^+-ATPase acted together with K^+/H^+ symporters. Here, the pumped H^+ was electrically compensated by a combined K^+/H^+ influx (Figure 1, C and D). The net K^+ influx shifted E_K to more negative voltages and thus also the zero-current voltage of the symporter, $E_{K/Hs}$. This shifted the membrane voltage at which the positive and negative electrical fluxes compensated each other to more negative values. Similar to case 1, the system had only one possible steady state determined by the equilibrium voltage of the H^+-ATPase: $I_P(V) = 0$, which implied $V = V_{0,pump}$, and $E_K = 2 \cdot V_{0,pump} - E_H$. Under this condition, the K^+/H^+ flux via the symporter was zero. With $pH_{cyt} = 7.0$, $pH_{apo} = 6.0$, and $V_{0,pump} = -200$ mV, the internal concentration would have equilibrated in this system at $[K^+]_{cyt} = 9 \times 10^5$ mM for $[K^+]_{apo} = 10\ \mu M$, and at $[K^+]_{cyt} = 9 \times 10^7$ mM for $[K^+]_{apo} = 1$ mM. Of course, these values are purely theoretical and are intended to illustrate how far the modeled scenario is from a physiological situation. The exorbitant gradients declined to still huge $[K^+]_{apo} = 10\ \mu M/[K^+]_{cyt} = 2{,}200$ mM and $[K^+]_{apo} = 1$ mM/$[K^+]_{cyt} = 2.2 \times 10^5$ mM, when setting $V_{0,pump} = -125$ mV in order to simulate energy consumption by other transport processes (see case 1). Here, a control of V or E_K by varying the K^+/H^+ symporter activity was not possible. Thus, a system of a pump and K^+/H^+ symporter is even more susceptible to K^+ overaccumulation than a "pump & channel" system (case 1).

Case 3: Only K^+/H^+ antiporters

A third 'what-if' scenario considered a case in which the proton H^+-ATPase acted together with K^+/H^+ antiporters that exchanged one K^+ for nH^+. An electroneutral K^+/H^+ antiport was represented by $n = 1$, and an electrogenic antiport by $n > 1$. The system with an electroneutral K^+/H^+ antiporter released K^+ until the K^+ gradient equaled the H^+ gradient ($E_K = E_H$). This release was energized by the proton gradient. The steady-state membrane voltage was $V_{0,pump}$, at which level no net ion flux occurred. In case of an electrogenic K^+/H^+ antiporter, the released K^+ ion was

electrically compensated by one inflowing H^+, while the other protons transported by the antiporter were electrically compensated by protons pumped out of the cell by the H^+-ATPase. The net proton fluxes were compensated by biochemical/metabolic processes (Sanders and Slayman, 1982; Wegner and Shabala, 2020; Wegner et al., 2021), whereas the release of K^+ shifted E_K positively along the voltage axis (Figure 1, E and F). A steady state was achieved only if $I_P(V) = 0$, which implied $V = V_{0,pump}$ and $E_{H/Ka} = V_{0,pump}$. Thus, in steady state, $E_K = n{\cdot}E_H{-}(n{-}1){\cdot}V_{0,pump}$. With this value, the K^+/H^+ flux via the antiporter was zero at $V_{0,pump}$. Considering the hypothetical case $n = 2$, the internal concentration would have equilibrated for $pH_{cyt} = 7.0$, $pH_{apo} = 6.0$, and $V_{0,pump} = -200$ mV at $[K^+]_{cyt} = 3.4 \times 10^{-8}$ mM for $[K^+]_{apo} = 10$ µM, and at $[K^+]_{cyt} = 3.4 \times 10^{-6}$ mM for $[K^+]_{apo} = 1$ mM. In an example of energy consumption by other transport processes (simulated by $V_{0,pump} = -125$ mV), the gradients would be $[K^+]_{apo} = 10$ µM/$[K^+]_{cyt} = 6.7 \times 10^{-7}$ mM and $[K^+]_{apo} = 1$ mM/$[K^+]_{cyt} = 6.7 \times 10^{-5}$ mM. As in the cases before, a control of V or E_K by varying the K^+/H^+ antiporter activity was not possible.

A first interim conclusion

The considerations presented in cases 1–3 allowed already a very fundamental conclusion: an isolated, static cell could not flexibly adjust E_K with a single K^+ transporter type. The steady state was always determined by the type of transport process, the transmembrane pH gradient, and the H^+-ATPase-dependent energy available for the K^+ transport process (represented by $V_{0,pump}$ in the model). The steady state varied between extremely low and extremely high unphysiological values, indicating that these simple K^+ transport modules are not (or are only conditionally) suitable for a well-regulated K^+ homeostasis at the plasma membrane. In the following, we examined how a mixture of different K^+ transporters could increase the cellular flexibility.

Case 4: Electroneutral and electrogenic K^+/H^+ antiporters

In a fourth 'what-if' scenario, the proton H^+-ATPase was combined with both electroneutral and electrogenic K^+/H^+ antiporters at the same time. The system established a steady state in which the H^+-ATPase pumped protons out of the cell and the electrogenic K^+/H^+ antiporter allowed the influx of two or more protons for the efflux of a K^+ ion, while the electroneutral K^+/H^+ antiporter released a proton in exchange for the uptake of a K^+ ion (Figure 2A). Thus, apparently futile K^+ and H^+ cycles dissipated valuable energy provided by ATP-hydrolysis at the pump. However, the cell could now adjust E_K and the membrane voltage by fine-tuning activity of the transporters (Figure 2, B and C).

A comprehensive analysis of the steady-state condition revealed that, compared to cases 1–3, which were characterized by exactly one steady state for E_K and V irrespective of the transporter activities (Figure 3A), case 4 enabled a larger spectrum of possible E_K–V couples (Figure 3B). Nevertheless, in this system E_K was always more positive than E_H (Figure 3B), which would still result in very low cytosolic K^+ concentrations under otherwise physiological conditions.

Case 5: K^+ channels and K^+/H^+ symporters

A fifth 'what-if' scenario considered a case in which the proton H^+-ATPase acted together with K^+ channels and K^+/H^+ symporters. In this system, a steady state was established in which the H^+-ATPase pumped a proton out of the cell, the K^+/H^+ symporter allowed the combined influx of a proton and a K^+ ion, while the channel released a K^+ ion (Figure 2D). Here, the combination of different K^+ transporter types established H^+ and K^+ cycles that were energized by the H^+-ATPase. This drawback, however, was compensated by the flexibility to adjust V and E_K by modifying transporter activity (Figure 2, E and F). Nevertheless, this flexibility still had its limits. The system considered in case 5 could only achieve a steady state in which $E_K < V$ (Figure 3C). Under this condition, an open potassium channel, regardless of its gating properties, released K^+ from the cell. If in the extreme case the probability of the K^+ channel being open was zero, that is, $p_o(V) = 0$, case 5 converted into case 2, in which $V = V_{0,pump}$ and $E_K = 2V_{0,pump}{-}E_H$.

Case 6: K^+ channels and K^+/H^+ antiporters

A sixth 'what-if' scenario considered a case in which the proton H^+-ATPase acted together with K^+ channels and K^+/H^+ antiporters. An electroneutral K^+/nH^+ antiport was represented by $n = 1$, and an electrogenic antiport by $n > 1$. The system established a steady state in which the H^+-ATPase pumped n protons out of the cell, while the K^+/H^+ antiporter exchanged n inflowing protons for an outflowing K^+ ion, which was reabsorbed by the potassium channel (Figure 2G). E_K and V could be flexibly fine-tuned by adjusting the transporter/channel activities (Figure 2, H and I). Greater antiporter activity increased both E_K and V, while greater channel activity increased V and decreased E_K. However, E_K was always positive of V in steady state (Figure 3, D–F). With increasing channel activity, the gap between V and E_K got smaller, while it got larger with increasing K^+/H^+ antiporter activity. If the K^+/H^+ antiporter was electroneutral (case 6a) E_K was never more positive than E_H (Figure 3D). If it was electrogenic (case 6b), the upper limit of E_K was $n{\cdot}E_H$-V (Figure 3E), which is physiologically irrelevant at the plasma membrane. In the physiological range, the main difference between both options was that the maintenance of the H^+ and K^+ cycles costed more energy with electrogenic antiporters. The combined presence of electrogenic and electroneutral antiporters (case 6c) did not produce evident new features (Figure 3F) compared to case 6b.

Case 7: K^+/H^+ symporters and K^+/H^+ antiporters

A seventh 'what-if' scenario considered a case in which the proton H^+-ATPase acted together with K^+/H^+ symporters and electroneutral or electrogenic K^+/H^+ antiporters. An

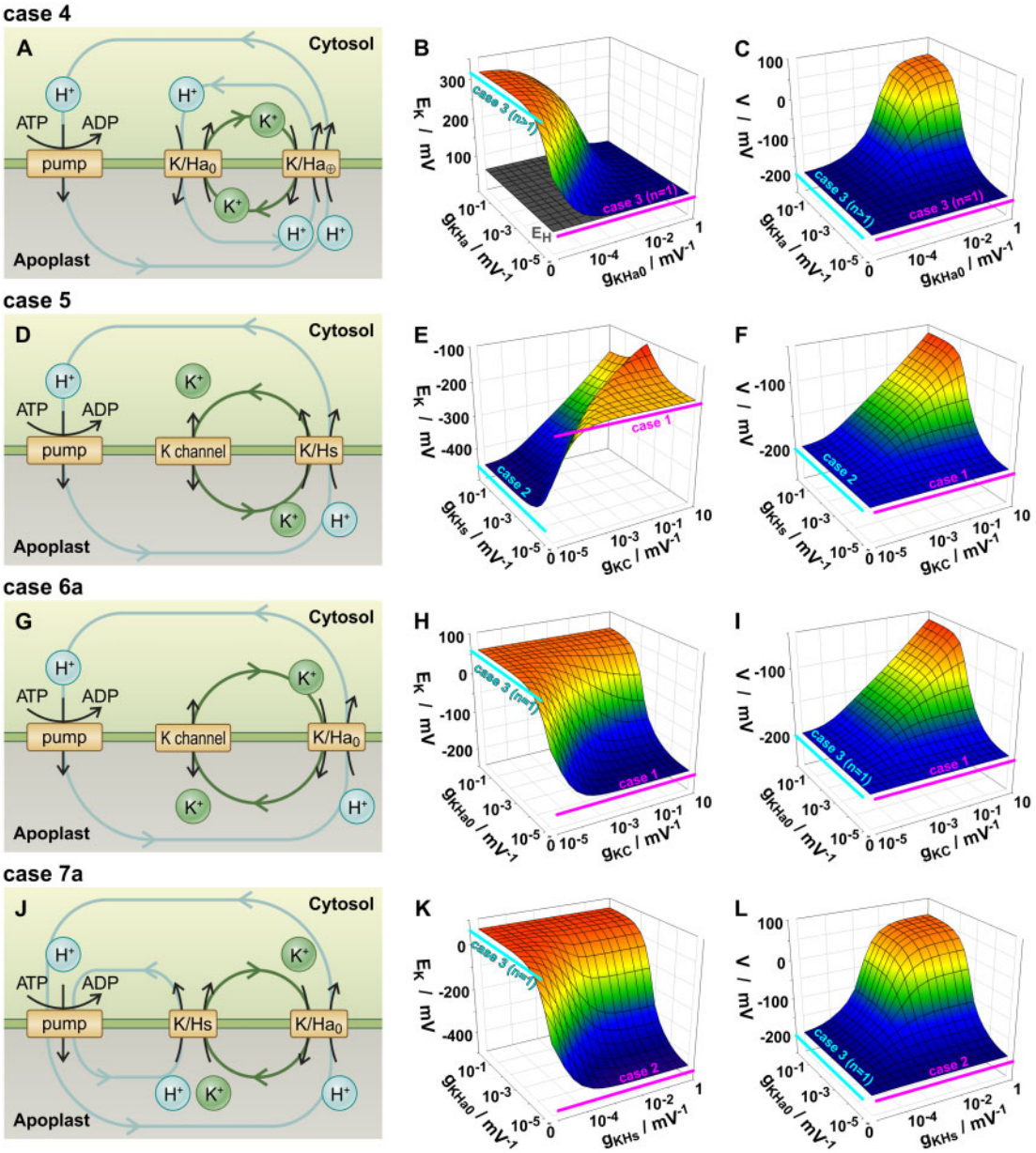

Figure 2 E_K and V as adjusted by pairs of K^+ transporters and the H^+ pump. A–C, Case 4. When electroneutral and electrogenic K^+/H^+ antiporters act together with the H^+-pump, three cycles establish in steady state: (i, green cycle) the electrogenic K^+/H^+ antiporter releases K^+, which is reabsorbed by the electroneutral antiporter; (ii and iii, blue cycles) a proton is released by the electroneutral antiporter (ii), which is reabsorbed by the electrogenic antiporter together with the H^+ released by the pump (iii). By modifying the transporter activities, the steady state of E_K (B) and V (C) can be freely adjusted within a certain range. For comparison, the respective steady states for the systems with only one K^+ transporter-type are indicated: only electrogenic K^+/H^+ antiporters ($g_{KHa0} = 0$; case 3, $n > 1$, cyan lines) and only electroneutral K^+/H^+ antiporters ($g_{KHa} = 0$; case 3, $n = 1$, magenta lines). D–F, Case 5. When K^+ channels and K^+/H^+ symporters act together with the H^+-pump, two cycles establish in steady state: (i, green cycle) the K^+ channel releases K^+, which is reabsorbed by the symporter together with the H^+ released by the pump (ii, blue cycle). By modifying the transporter activities, the steady state of E_K (E) and V (F) can be freely adjusted within a certain range. For comparison, the respective steady states for the systems with only one K^+ transporter-type are indicated: only K^+/H^+ symporters ($g_{KC} = 0$; case 2, cyan lines) and just K^+ channels ($g_{KHs} = 0$; case 1, magenta lines). G–I, Case 6a. When K^+ channels and K^+/H^+ antiporters act together with the H^+-pump, two cycles establish in steady state: (i, green cycle) the K^+ channel absorbs K^+, which is released by the antiporter; (ii, blue cycle) the H^+ released by the pump is absorbed by the antiporter. By modifying the transporter activities, the steady state of E_K (H) and V (I) can be freely adjusted within a certain range. For comparison, the respective steady states for the systems with only one K^+ transporter-type are indicated: only electroneutral K^+/H^+ antiporters ($g_{KC} = 0$; case 3, $n = 1$, cyan lines) and only K^+ channels ($g_{KHa0} = 0$; case 1, magenta lines). J–L, Case 7a. When K^+/H^+ symporters and K^+/H^+ antiporters act together with the H^+-pump, three cycles establish in steady state: (i, green cycle) the symporter absorbs K^+, which is released by the antiporter; (ii, inner blue cycle) a proton released by the pump is absorbed by the symporter, (iii, outer blue cycle) while another released proton is absorbed by the antiporter. By modifying the transporter activities, the steady state E_K (K) and V (L) can be freely adjusted within a certain range. For comparison, the respective steady states for the systems with only one K^+ transporter-type are indicated: only electroneutral K^+/H^+ antiporters ($g_{KHs} = 0$; case 3, $n = 1$, cyan lines) and only K^+/H^+ symporters ($g_{KHa0} = 0$; case 2, magenta lines).

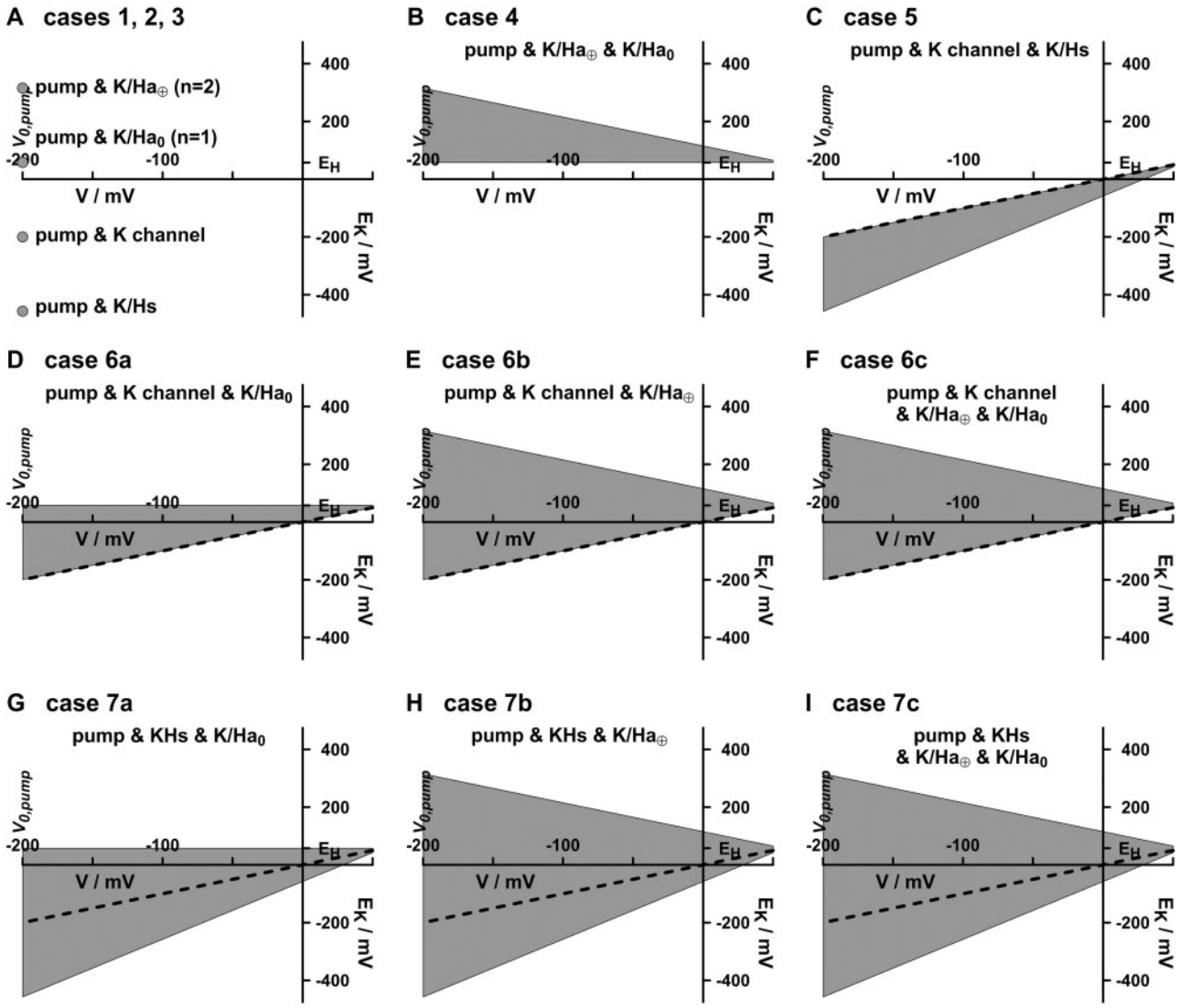

Figure 3 Accessible E_K–V ranges for the different K^+ transporter combinations exemplarily shown for $V_{0,pump} = -200$ mV. A, With a single transporter type, only one steady-state condition is achievable, which is independent of the transporter activity (grey dots for the different cases). B–I, The combination of transporter types enables steady states in a wider range (grey areas) by adjusting the activities of the transporters. Nevertheless, there are still limitations. For better orientation, the dashed lines indicate where $E_K = V$. The upper limits in (B, E, F, H, I) are determined by $E_K \leq n \cdot E_H - (n-1) \cdot V$, in (C) by $E_K \leq V$, and in (D, G) by $E_K \leq E_H$. The lower limits in (B) are $E_K \geq E_H$, in (C, G, H, I) $E_K \geq 2 \cdot V - E_H$, and in (D–F) $E_K \geq V$.

electroneutral K^+/nH^+ antiport was represented by $n = 1$, and an electrogenic antiport by $n > 1$. The system established a steady state, in which the H^+-ATPase pumped $(n + 1)$ protons out of the cell, while the K^+/H^+ antiporter exchanged n inflowing protons for one outflowing K^+ ion, which was reabsorbed together with a proton by the K^+/H^+ symporter (Figure 2J). The behavior of the system in response to changes of the transporter activities was very similar to case 6. E_K and V could be flexibly fine-tuned by adjusting the transporter activities (Figure 2, K and L). Greater antiporter activity increased both E_K and V, while greater symporter activity increased V and decreased E_K. Compared to cases 5 and 6, however, the system of case 7 gained another level of flexibility. While in case 5 E_K was always more negative than the membrane voltage V (Figure 3C), and in case 6 E_K was always more positive than V (Figure 3, D–F), in case 7 E_K could be adjusted in both ranges (Figure 3, G–I).

Case 8: K^+ channels, K^+/H^+ symporters and K^+/H^+ antiporters

In an eighth 'what-if' scenario, all different K^+ transporter types were combined. This system showed the total composite complexity of all other systems previously considered, but did not go beyond. E_K and V could be flexibly adjusted within the same limits as in case 7 by fine-tuning the transporter activities (Figure 4). This flexibility was again at the cost of energy-consuming K^+ and H^+ cycles. For systems with electrogenic K^+/H^+ antiporters, the energy costs were higher than for systems with electroneutral antiporters.

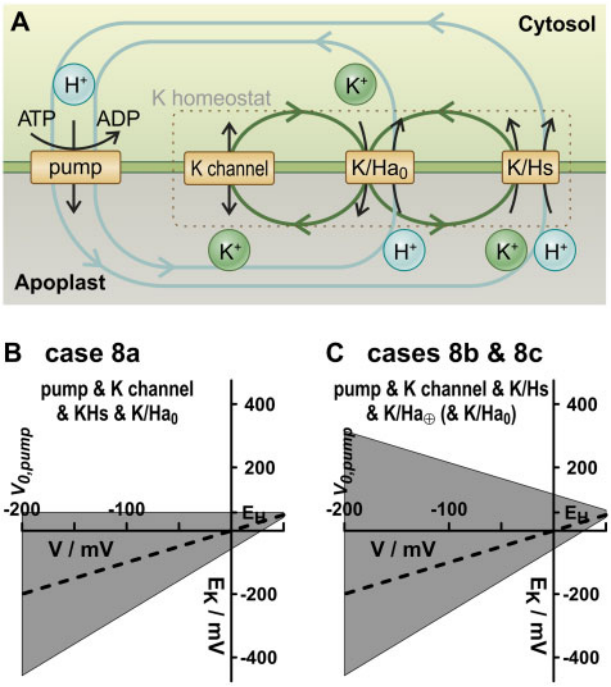

Figure 4 Flexibility of a system with different types of K^+ transporters. A, Energized by the H^+-ATPase, the K homeostat (consisting of K^+ channels, K^+/H^+ symporters and K^+/H^+ antiporters, items enclosed by grey dashed line) exhibits four cycles that aggregate in two patterns. A proton that is released by the pump is reabsorbed by the antiporter in exchange for a released K^+, which in turn is reabsorbed (i) either by the channel or (ii) together with another proton by the symporter. Colored cycles represent flow of the respective colored ion. B and C, By adjusting the transporter activity, a large range of E_K–V steady states can be achieved (grey areas). B, With electroneutral antiporters, the range is limited to $E_K \leq E_H$. C, With electrogenic antiporters, these limits are further extended to more positive values [$E_K \leq n \cdot E_H - (n-1) \cdot V$]. The dashed lines indicate where $E_K = V$.

Case 9: Anion channels

After the inventory of the effects of K^+ transporters, the consequences of charge-balancing anions were considered, first alone and later in combination with the K^+ transporters. The ninth 'what-if' scenario considered a case in which the proton H^+-ATPase acted together with anion channels. In such a system, the positive proton pump current was compensated by an efflux of anions (Supplemental Figure S1, A and B). The release of A^- led to a negative shift of E_A, which also negatively shifted the voltage at which the H^+ efflux compensated the A^- efflux. A stable steady state could be reached in this system only if $I_P(V) = 0$ and $E_A = V$. This means that the membrane voltage adjusted to the steady-state voltage of the H^+-ATPase, and also that E_A was fixed to this value, causing there to be neither a net A^- flux via the channel nor a net H^+ flux via the pump. Under the conditions presented above ($pH_{cyt} = 7.0$, $pH_{apo} = 6.0$; $V_{0,pump} = -200$ mV), a steady-state condition would be $[A^-]_{apo} = 1\ mM/[A^-]_{cyt} = 3.4 \times 10^{-4}$ mM. If other transport processes consumed part of the energy provided by the pump (simulated by setting $V_{0,pump} = -125$ mV), the steady state would be $[A^-]_{apo} = 1\ mM/[A^-]_{cyt} = 6.7 \times 10^{-3}$ mM, thus still unphysiologically low. As in the cases 1–3 of single K^+ transporters, the steady-state values in case 9 could not be influenced by changing the anion channel activity.

Case 10: H^+/A^- symporters

A 10th 'what-if' scenario considered a case in which the proton H^+-ATPase acted together with H^+/A^- symporters. Here, the pumped H^+ was electrically compensated by a combined $2H^+/1A^-$ influx (Supplemental Figure S1, C and D). While the net proton fluxes were balanced by metabolic/biochemical processes (Sanders and Slayman, 1982; Wegner and Shabala, 2020; Wegner et al., 2021), the uptake of anions shifted E_A positively along the voltage axis and decreased the zero-current voltage of the symporter, $E_{H/A}$. As a consequence, the membrane voltage at which the positive and negative electrical fluxes compensated each other also shifted to more negative values. The system had only one possible steady state at $V = V_{0,pump}$, which implied $E_A = 2 \cdot E_H - V_{0,pump}$. Under this condition, the net H^+/A^- flux via the symporter was zero. Considering again the exemplary conditions used above ($pH_{cyt} = 7.0$, $pH_{apo} = 6.0$, and $V_{0,pump} = -200$ mV), this system would have equilibrated at $[A^-]_{cyt} = 3 \times 10^5$ mM for $[A^-]_{apo} = 1$ mM. When setting $V_{0,pump} = -125$ mV to simulate energy consumption by other transport processes, the gradient would still be $[A^-]_{cyt} = 1.5 \times 10^4$ mM for $[A^-]_{apo} = 1$ mM. Here, a control of V or E_A by varying the H^+/A^- symporter activity was not possible. Thus, symporters alone would generate very high $[A^-]_{cyt}$ (very positive E_A), while anion channels alone would cause very low $[A^-]_{cyt}$ (very negative E_A).

Case 11: A^- channels and H^+/A^- symporters

Next, the combination of anion channels and $2H^+/A^-$ symporters was tested in the 11th 'what-if' scenario (Figure 5). As in the cases of the combinations of potassium transporters, the presence of different anion transporters in the network now allowed the cell to flexibly adjust E_A and V within certain ranges by changing the transporter activities. This gain in flexibility was again at the cost of anion and H^+ cycles. An anion that was released from the cell was reabsorbed together with two protons via the symporter. To energize this cycle, the two protons were pumped out of the cell by the H^+-ATPase.

Cases 12–16: One homeostat in combination with a single transporter

To understand how the combination of K^+ and A^- transporters effected the homeostatic control of the respective other ion, the two anion transporters ("A-homeostat") were combined with the pump and with one of each of the three K^+ transporter types (case 12: K^+ channel, case 13: K^+/H^+ symporter, case 14: K^+/H^+ antiporter). The "K-homeostat" (K^+ channel, K^+/H^+ symporter and $1K^+/1H^+$ antiporter) was combined with the pump and either the anion channel (case 15) or the H/A symporter (case 16; Supplemental

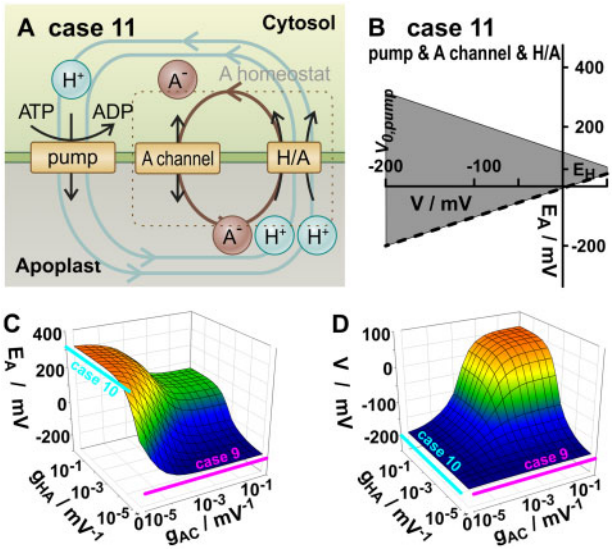

Figure 5 Flexibility of a system with different types of A^- transporters (case 11). A, Energized by the H^+-ATPase, the A homeostat (items enclosed by the grey dashed line), consisting of anion channels and electrogenic H^+/anion symporters, exhibits three cycles. Two protons that are released by the pump are reabsorbed by the symporter together with an anion, which in turn is released by the channel. Colored cycles represent flow of the respective colored ion. B, By adjusting the transporter activity, a large range of E_A–V steady states can be achieved (grey areas). The dashed line indicates where $E_A = V$. C and D, By modifying the transporter activities, the steady state of E_A (C) and V (D) can be freely adjusted within a certain range. For comparison, the respective steady states for the systems with only one A^- transporter-type are indicated: only A^- channels ($g_{HA} = 0$; case 9, magenta lines) and only $2H^+/1A^-$ symporters ($g_{AC} = 0$; case 10, cyan lines).

Figure S2). In all these cases, the respective homeostat determined V, the steady-state membrane voltage and the concentration gradient of the particular substance (E_K for K-homeostat, E_A for A-homeostat). Varying the activity of the single transporters neither influenced E_K nor E_A (Supplemental Figure S2). The E_K and E_A values, respectively, were fixed in steady state to the prevailing membrane voltage as shown in cases 1–3, 9, and 10. In cases 12–16, the cycles of the respective homeostat consumed part of the electrochemical energy provided by the H^+-ATPase, which manifested in the difference between V and $V_{0,pump}$. As noted above, in some examples for cases 1, 2, 3, 9, and 10, the same effect was simulated by modifying $V_{0,pump}$ to clamp a different membrane voltage.

Case 17: K-homeostat and A-homeostat

When instead of single transporters, both homeostats were combined (case 17; Supplemental Figure S3) the system gained the full flexible range of controlling E_K and E_A. Variations in the activity of a K^+ transporter affected not only the steady state of E_K, but also the membrane voltage V and, via V, the steady state of E_A. In the same way, variations in the activity of an anion transporter directly affected both E_A and V and, via V, also E_K. Nevertheless, the orientation of E_K toward V was exclusively determined by the K transporters while the orientation of E_A toward V was only fixed by the anion transporters. In other words, only the corresponding homeostat was able to set whether (1) $V-E_X > 0$, (2) $V-E_X = 0$, or (3) $V-E_X < 0$. Variations in the other homeostat could not cause a switch between these three possibilities.

Cases 18–20: K-homeostat and sugar transporters

After having systematically analyzed transporter networks for cations and for anions alone and in combination, the transport of an electrically neutral nutrient was elaborated next. For this purpose, the H^+-ATPase and the K-homeostat (comprising K^+ channels, K^+/H^+ symporters and electroneutral K^+/H^+ antiporters) were combined in a 18th 'what-if' scenario with proton-coupled sugar transporters (H/C), in a 19th scenario with sugar uniporters (SWEETs) and in an 20th with both sugar transporter types (Figure 6). For simplicity, the A-homeostat was not included. As previously shown, its presence would influence the transport of K^+ and sugar only by consuming part of the cellular energy, which would manifest in a different steady-state value of V. Such an effect could also be simulated by other processes, such as adjusting $V_{0,pump}$ or allowing the K-homeostat to consume more energy.

To illustrate the effects of the sugar transporters, the different parameters of the K-homeostat were set to achieve a steady state of $V \approx -175$ mV and $E_K \approx -117$ mV in the absence of any sugar transporter, and were kept constant in all scenarios 18–20. Different parameters would not have qualitatively changed the results. In the presence of proton-coupled sugar transporters alone (case 18), V and E_K did not change, irrespective of the activity of the H/C transporter (Figure 6, A–D, case 18, magenta). Also, the sugar concentration gradient was independent of whether H/C was moderately or highly active. The steady-state value was always $[C]_{cyt} \approx 1.1 \times 10^4 \cdot [C]_{apo}$, and was determined by the pH gradient and the membrane voltage $[\ln([C]_{apo}/[C]_{cyt}) = F/(RT) \cdot (V\text{-}E_H)]$. When the proton-coupled sugar transporter was replaced by a sugar uniporter (case 19), this steady-state gradient collapsed to $[C]_{cyt} = [C]_{apo}$. In this case, neither the sugar gradient, nor E_K, nor V were affected by changing the uniporter activity (Figure 6, A–D; case 19, cyan). If, however, both transporter types were simultaneously in the membrane, the system became sensitive toward changes in the transporter activities. The presence of both transporter types established an apparently futile C-cycle that consumed cellular energy. As a consequence, V increased with increasing sugar cycling, and this changed the driving-force for ions, affecting E_K as well (Figure 6, A–D; case 20). Thus, adjusting the sugar gradient by fine-tuning the activity of the sugar transporters also affected K^+ homeostasis via the energy status of the cell. Interestingly, the same thought experiments with only one active K^+ transporter at a time reproduced cases 1 ($E_K = V$), 2 ($E_K = 2 \cdot V - E_H$), and 3 ($E_K = E_H$). In these cases, the steady-state voltage V was less negative the

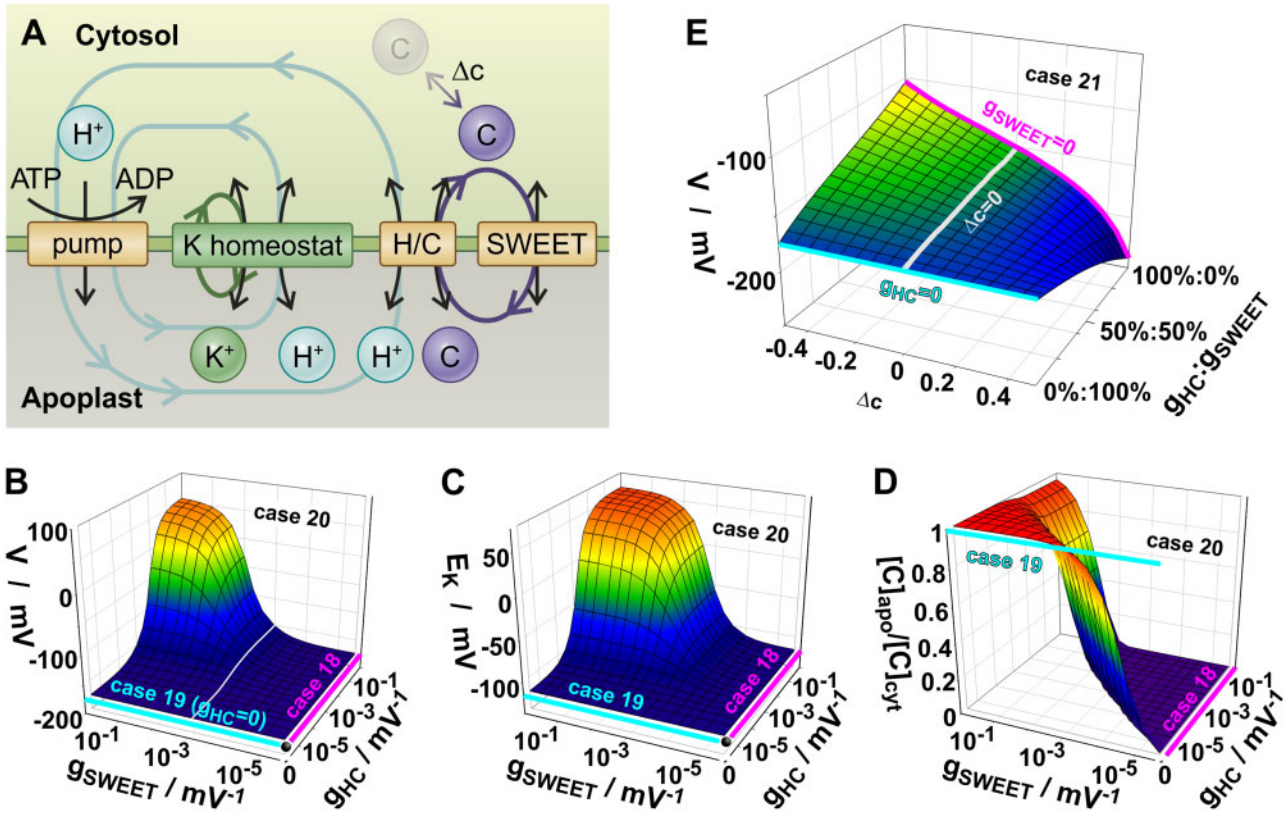

Figure 6 Combination of K^+ and sugar transport. The K-homeostat (Figure 4) was combined with sugar transport via uniporters (SWEET) and/or proton-coupled symporters. A, In addition to the cycles of the K-homeostat, the presence of both sugar transporter types established proton/sugar cycles, in which a sugar molecule is released by SWEET and reabsorbed by the symporter together with a proton that is released by the pump. Colored cycles represent the flow of the respective colored ion/metabolite. In addition, the metabolization of sugar was also simulated (Δc). B–D, When both sugar transporters are present (case 20), the membrane voltage (B) and the transmembrane sugar gradient (D) can be adjusted by fine-tuning the transporter activities. The altered energetic status of the cell indicated by the steady-state voltage V (B) also affected E_K (C). When only one sugar transporter type is present (case 18: only H/C; case 19: only SWEET) the activity of the transporter does not affect V, E_K or the sugar gradient in steady state (magenta and cyan lines). E, Case 21. Effect of metabolic sugar production ($\Delta c > 0$) or sugar consumption ($\Delta c < 0$) on the steady-state membrane voltage V. An effect was only observable in the presence of electrogenic H/C transporters. If only electroneutral SWEETs were present, sugar metabolism did not affect V (cyan line). The white line indicates $\Delta c = 0$ and follows the white trajectory in (B).

more energy the sugar cycle consumed. Therefore, to adjust K^+ and sugar gradients independently of each other, two different transporter types for each substrate were needed in the membrane, resulting, consequently, in cycles for K^+ and sugar.

Case 21: Metabolism can affect the energetics of membrane transport

In the same system as before, the influence of metabolic processes on the homeostatic conditions was tested. For this purpose, the production ($\Delta c > 0$) or consumption ($\Delta c < 0$) of cytosolic sugars was simulated (Figure 6A). Without any sugar transporter in the membrane, the K-homeostat was not affected at all by metabolic changes of the sugar concentration. Similarly, when only electroneutral sugar uniporters were present, sugar production or consumption affected only the transmembrane sugar gradient but had no effect on the steady-state membrane voltage V (Figure 6E, cyan) or E_K. However, in the presence of electrogenic proton-coupled sugar transporters, sugar metabolism affected the membrane voltage (Figure 6E) and, via this, E_K. Compared to the conditions without metabolism, sugar production increased the transmembrane sugar gradient, which resulted in additional efflux via sugar uniporters and sugar–proton symporters. Although the electroneutral transport via uniporters did not affect the membrane voltage, the electrogenic transport via proton-coupled transporters provoked a more negative V. Conversely, sugar consumption led to an additional sugar gradient into the cell, which resulted in additional sugar influx. When mediated by proton-coupled symporters, this influx provoked a less negative V (Figure 6E). Thus, if metabolic processes are coupled to electrogenic transport processes, they can interfere with general homeostatic control.

Generalization for more nutrients

In further iterative steps, the transporter system could be brought successively closer to a real physiological situation. K^+ transporters and sugar transporters could be combined into a new "K/C homeostat", which would then be combined with transporters for another nutrient or ion. The conclusions drawn before for sugar transport would then be valid for the new substrate. The different homeostat modules were largely independent of each other but coupled via the energetic status of the cell. A special case that needs to be investigated in a separate study, however, would be flux coupling in one transporter, which may occur with Na^+ and K^+ in HKT channels (Riedelsberger et al., 2019, 2021).

Cases 22: Symplastic diffusion

All the scenarios so far considered a static isolated cell. The reality in a plant, however, is more complex. For instance, cells are connected to neighbors via plasmodesmata, enabling intercellular diffusion. This process could be covered in the model by a mathematical description similar to case 21. A loss of nutrients by diffusion to a neighboring cell was equivalent to a transport process out of the cell, while a diffusive gain of nutrients was equivalent to a transport process into the cell. For exemplary illustration, the transporter network of case 12 (Supplemental Figure S2A) was considered again in a 22nd 'what-if' scenario extended with these diffusion processes (Supplemental Figure S4). Without diffusion, E_K was identical to the steady-state membrane voltage, irrespective of the activity of the K^+ channel. Likewise, E_A was constant in all these conditions. Diffusion out of the cell did not markedly influence V, caused a moderate decline of E_A, but strongly affected E_K, provoking $E_K > V$. The latter effect was more pronounced the lower the K^+ channel activity was; thus, the less loss by diffusion could be compensated by uptake. Diffusion into the cell had the opposite effects. Diffusion could therefore be considered as an additional transport process with which a cell gained flexibility to adjust E_K, even with a single membrane transporter type for K^+, in this case, a K^+ channel. In a normal physiological condition, however, g_{KC} is on the order of magnitude of 10^{-1} mV^{-1}, suggesting that the influence of diffusion on homeostatic conditions is not strong. Additionally, if the diffusion process stops because plasmodesmata close or because a symplastic concentration gradient is missing, even a symplastically connected cell is not different from cases 1–21 with all the consequences described above.

Case 23: Volume changes

In principle, volume changes could also affect homeostatic processes. During stomatal movement, for instance, a guard cell increases its volume by ~25% and its surface area by ~15% (Meckel et al., 2007; Jezek and Blatt, 2017). Compared to a static cell as was considered so far, the increased volume would imply a dilution of the cytosolic nutrient concentrations and the increased surface area would imply an increased electrical capacitance of the membrane, which in turn would result in a reduction of the magnitude of membrane voltage. To estimate the impact of these effects, they were included in the mathematical description (Supplementary Equations S1 and S2) and were exemplarily simulated in a 23rd 'what-if' scenario (Figure S5), which is based on cases 12 and 22. To estimate the parameter range, we considered a guard cell that changed rather rapidly in a linear manner from 4 pl and 20 pF (closed) to 5 pl and 23 pF (open) in 60 min (Hosy et al., 2003). From these values and with exemplarily chosen values $V \approx -100$ mV, $I_{max} = 20$ pA, and $[K^+]_{cyt} = 100$ mM, the orders of magnitude of $\gamma = -V/I_{max} \cdot dC/dt \approx 4 \times 10^{-6}$ and $\Delta k = -e_0/I_{max} \cdot N_A \cdot [K^+]_{cyt} \cdot dVol/dt \approx -0.15$ were calculated. Slower stomatal movements would result in even lower values. In comparison to the membrane transport processes (e.g. a usual value for i_p, Supplemental Equation S1, is in the range of 0.2–0.7), the contribution of the parameter γ is negligible. The change of the volume, however, could influence the homeostatic conditions (Figure S5B), similar to case 22. Nevertheless, each guard cell will sooner or later reach its maximal or minimal expansion ($dVol/dt = 0$), and for these conditions, cases 1–21 also apply to guard cells.

Homeostasis in organelles

Up to now, the problem of homeostasis has been addressed at a single membrane. The presented results were exemplarily obtained for the plasma membrane. But they can be adapted in a similar manner to the vacuolar membrane or any other organelle membrane (Figure 7A). In the cellular context, however, these membranes are not isolated. Instead they communicate with each other via the cytosolic (i.e. their external) concentrations (Vincent et al., 2017; Horaruang et al., 2020). Previous studies have shown that membrane sandwiches exhibit another level of dynamics (Gajdanowicz et al., 2011; Schott et al., 2016; Dreyer et al., 2017, 2019). Therefore, nutrient homeostasis was also investigated with respect to these dynamics. It turned out that cytosolic concentrations could remain equilibrated in two different modes. In a long-term stable steady state, the net-fluxes of each substrate across each membrane separately were zero (Figure 7A), while on a much shorter time scale, the shuttling of nutrients from the lumen of an organelle to the apoplast and/or vice versa was also possible (Figure 7, B–E). The first mode implied the presence of energy-consuming nutrient cycles. The second mode may function without such cycles. However, it was not stable in the long-term because the nutrient net-fluxes changed the nutrient concentrations, particularly in the lumen, which is an enclosed compartment without additional inlets and outlets. Furthermore, the nutrient concentrations in the apoplast could change. However, in that case, diffusion processes may partially mitigate this effect. Importantly, the changed concentrations reduced the driving forces for the fluxes. In the end, every possible arrangement of the second mode (Figure 7, B–E) resulted in the long-term stable-steady state of the first mode (Figure 7A). Thus, the processes investigated in this study are not special cases, but a fundamental basis of nutrient homeostasis in plant cells.

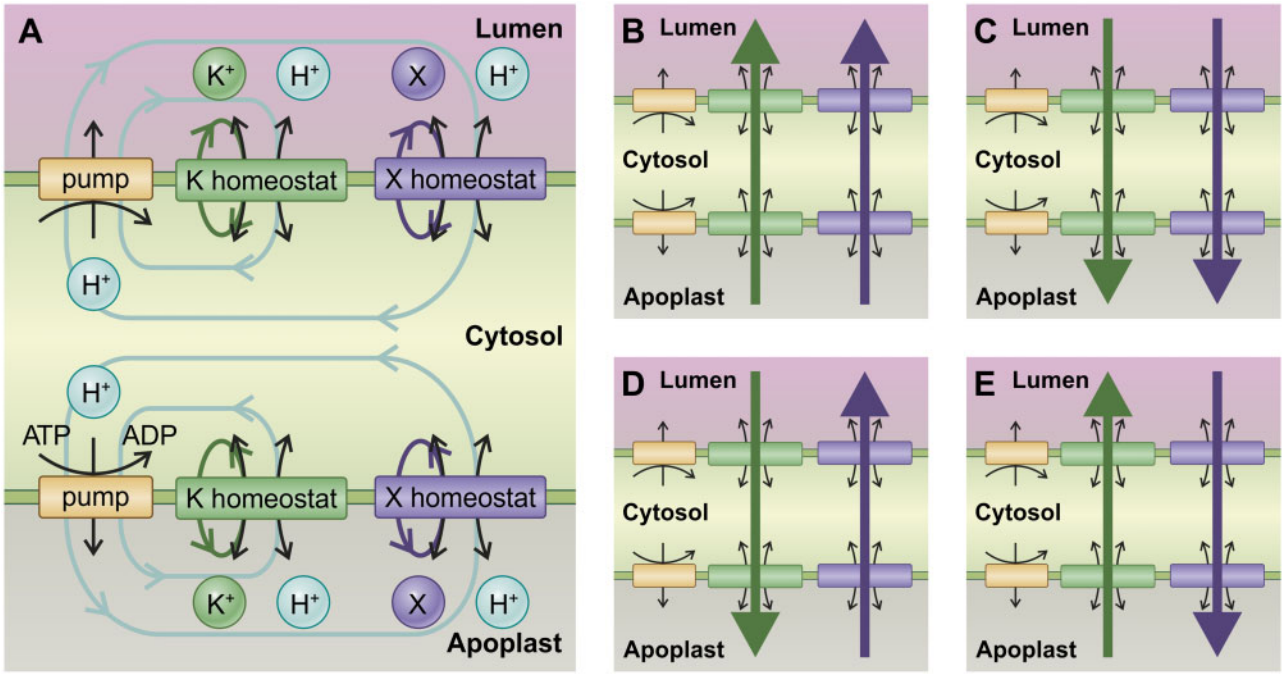

Figure 7 Combination of homeostats in membrane sandwiches. A, Homeostats at the plasma membrane and at organelle membranes may maintain constant cytosolic nutrient concentrations for a longer time by independently cycling the nutrients across the different membranes. Colored cycles represent flow of the respective colored ion/nutrient. By adjusting the transporter activities, the concentrations and membrane voltages can be fine-tuned. B–E, Nutrients can be sequestered into or remobilized from organelles by shuttling them across the cytosol. Colored arrows represent the net fluxes of the respective colored ion/nutrient. For two different nutrients, the four possibilities of nutrient fluxes are shown. These systems are only temporarily in flux steady state, that is, constant fluxes, as the fluxes change concentrations in the lumen and the apoplast while cytosolic concentrations remain stable. On longer timescales, the systems (B–E) approach the situation displayed in (A).

Discussion

Transport processes across membranes are ruled by fundamental, well-understood laws. This allows researchers to describe them in mathematic terms (Beilby, 2007; Hills et al., 2012; Beilby and Al Khazaaly, 2016; Dreyer, 2017) and to run computational cell biology simulations. Such solidly based thought experiments have an inestimable value in gaining insights because simulations enable testing of conditions that are hard to achieve in conventional wet-laboratory experiments. The present study analyzed the basis of homeostasis and allowed far-reaching conclusions for our physiological understanding.

Two different transporter types are needed for homeostatic control

Comparison of cases 1–3 with 5–8, of cases 9 and 10 with 11, and of cases 18 and 19 with 20 showed that a cell gained flexibility by combining at least two different transporter types. Only then could the different E_X and V be adjusted in certain ranges by fine-tuning the transporter activities. This insight may explain why plants have different transporter types for many macronutrients. It is not that these transporters have different "affinities" and act in different concentration ranges (Dreyer and Michard, 2020). Instead, they act together and simultaneously, and thus can control the transmembrane concentration gradient in order to keep the cytosolic concentration constant even under varying external conditions. An important feature in this mechanism is that the transport through these transporter types is energized differently. For instance, one type of transporter operates along the electrochemical gradient of the nutrient while others use coupled nutrient and proton gradients as their driving force. Only the combination of these differently energized transport processes enables flexible control. In this context, other processes like diffusion or metabolism may also be considered as "transporter-equivalent." As indicated in scenarios 21, 22, and 23, such a process can replace, under certain conditions, one of the two necessary transporter types.

"Futile" nutrient cycles in plants are important for homeostasis

The flexibility to adjust V and E_X via two transporter types was inevitably linked to the presence of apparently futile nutrient cycles. Thus, these "futile" cycles are not as futile as they seem. Instead, they are important for the dynamic flexibility of the system. Nutrient cycling is a well-observed phenomenon in plants (Britto and Kronzucker, 2006), not only in normal conditions but, in particular, under salt stress (Munns et al., 2020; Shabala et al., 2020). Nutrient cycles were doubtlessly identified with radioactive tracers ($^{42}K^+$ and $^{13}NH_4^+$; Britto et al., 2001; Coskun et al., 2010, 2013) and often considered as an avoidable energy dissipation. This interpretation may suggest eliminating them in breeding programs. The fundamental insights provided here

may set a different spotlight on this issue. The elimination of "futile" cycles by silencing transporters will straightforwardly reduce the ability of the plant to maintain homeostatic control and will most likely come at the expense of fitness. The proton pump, together with the metabolically determined transmembrane pH gradient, provides strong steady driving forces for transport processes in plant cells. The examples presented in this study indicate that for a plant cell, a severe problem is not necessarily the uptake of a nutrient but its overaccumulation, particularly if it is a macronutrient. Nutrient cycles are a very elegant way out of this dilemma. They do not only allow the tight control of the cytosolic nutrient concentration but may also allow dissipation of excess energy, if needed, without having to shut down cellular energy production at a greater expense.

Alternative scenarios

The presented cycling scenario for K^+ homeostasis is a simple, rather intuitive conclusion from experimentally determined properties of membrane transporters. It should be mentioned, however, that in particular for guard cells, an average constant cytosolic [K^+] has been explained with a more complex alternative scenario. It was proposed that guard cells are unlikely to be found in a state in which the net flux of an osmotically active solute is zero. Instead, it was suggested that they transit between situations of osmotic solute uptake and loss, to achieve by time-averaged approximation a dynamic range of (quasi-)steady states of solute contents (Chen et al., 2012). These conclusions were drawn from observations of excised guard cells in epidermal strips that membrane voltage can spontaneously oscillate in an action potential (AP)-like behavior with periods from a few tens of seconds to many minutes (Thiel et al., 1992; Gradmann et al., 1993). These oscillations are between two quasi-stable states, a depolarized state associated with K^+ and Cl^- efflux, and a hyperpolarized state at which ion uptake is supposed to occur. Intriguingly, these spontaneous oscillations were not observed in guard cells in intact plants, although these cells can stay in the hyperpolarized state over longer time periods (Roelfsema et al., 2001) raising questions about how guard cells achieve K^+ homeostasis in vivo without oscillations, particularly when they are maximally swollen. K^+ cycling mediated by the K-homeostat (case 8) may provide an answer to this question.

K^+ homeostasis and electrical signaling

Instead of being a mechanism of homeostasis, the observed membrane potential oscillations in excised guard cells may be related to other physiological processes like APs, which are essential parts of electrical signaling in plants (Trebacz et al., 2006; Choi et al., 2016; Hedrich et al., 2016; Cuin et al., 2018; Gilroy et al., 2018; Farmer et al., 2020). Essential for APs is that excitable cells remain at a hyperpolarized resting voltage over a long period (Böhm et al., 2016; Iosip et al., 2020). Each spontaneous oscillation to release overaccumulated osmotically active ions, as K^+ and Cl^-, would fire an AP and would strongly distort electrical signaling. In the Venus flytrap (*Dionaea muscipula*), for instance, such spontaneous oscillations would cause false triggering of the trap mechanism (Scherzer et al., 2019). A trigger hair cell in Venus flytrap, as an example for an excitable cell, has to rest in a steady state with a reasonable negative membrane voltage until it gets mechanically stimulated to fire an AP. The resting membrane voltage V is determined by the activity of all ion transporters in the membrane and is in the range of $-200\ \text{mV} < V < -100\ \text{mV}$ (Scherzer et al., 2019; Iosip et al., 2020). Considering that K^+ and anions like Cl^- are the main players in the execution of plant APs (Beilby and Coster, 1979; Beilby and Walker, 1996; Beilby and Al Khazaaly, 2016, 2017; Cuin et al., 2018; Kisnieriene et al., 2019), such a condition could be achieved by a transporter network of case 17 or 12. While case 17 can flexibly realize all three possibilities (1) $V < E_K$, (2) $V = E_K$, or (3) $V > E_K$, case 12 is limited to $V = E_K$. In specific circumstances, with stable external [K^+] conditions, this could be sufficient. However, the limited flexibility would certainly be the weak point of such a system.

Conclusion

The comprehensive analysis of the dynamics of transporter systems suggests that nutrient cycles are important for homeostatic control. The elimination of these cycles by silencing transporters will likely decrease the fitness of the plant. To improve nutrient use efficiency in crops, different strategies are needed. One path could be the continuation with computational cell biology simulations and dry-lab experiments. This might provide further fundamental insight into the dynamics of the systems and may preserve us from too many dead-end strategies being tested in the wet-lab and in field trials. Predictably, we will not be able to create superplants that grow with excellent performance under a wide range of environmental conditions. Instead, it would make sense to use our growing experimental and theoretical knowledge of plant nutrient transport processes to design not only the plant but also the growth conditions so that the two are a perfect match.

Materials and methods

Mathematical description of transporter activities

H^+-ATPase

The voltage-dependent current of the H^+-ATPase was described with a mechanistic six-state pump model (Dreyer, 2017; Reyer et al., 2020) that pumps with a 1 H^+:1 ATP ratio (Blatt et al., 1990):

$$I_{HATPase}(V) = I_{max} \cdot i_P(V) = I_{max} \cdot \frac{1 - e^{\frac{-F}{RT}(V - V_{0,pump})}}{1 + e^{\frac{-F}{RT}(V + 135\text{mV})} + e^{\frac{-F}{RT}(0.1 \cdot V + 62.5\text{mV})}} \quad (1)$$

where, F is the Faraday constant, R is the gas constant, and T is the absolute temperature. I_{max} is the maximum current, which depends on the number of active pumps in the membrane and the cytosolic and apoplastic proton concentrations. $V_{0,pump}$ is the voltage at which the pump current is

zero. It depends on the cytosolic and apoplastic proton concentrations and on the cytosolic ATP, ADP, and Pi concentrations, that is, on the energy status of the cell (Rienmüller et al., 2012). In the examples presented in this study, this value was set exemplarily to $V_{0,pump} = -200$ mV; different values would not qualitatively change the results. In some examples, this parameter was modified to simulate the consumption of energy by other transport processes.

1 H^+:1 K^+ symporter

Proton ($J_{H,KHs}$) and potassium net flux ($J_{K,KHs}$) from the cell and the current–voltage relationship (I_{KHs}) of a 1:1 H^+-coupled K^+/H^+ symporter:

$$J_{H,KHs} = \frac{G_{KHs}}{e_0} \cdot (2 \cdot V - E_H - E_K) \quad (2)$$

$$J_{K,KHs} = \frac{G_{KHs}}{e_0} \cdot (2 \cdot V - E_H - E_K) \quad (3)$$

$$I_{KHs} = e_0 \cdot (J_{K,KHs} + J_{H,KHs}) = 2 \cdot G_{KHs} \cdot (2 \cdot V - E_H - E_K) \quad (4)$$

where, V is the membrane voltage, e_0 is the elementary charge, E_K is the Nernst voltage for potassium, and E_H is the Nernst voltage for protons. G_{KHs} is the membrane conductance of this transporter type (pA·mV^{-1}).

n H^+: 1 K^+ antiporter

Proton ($J_{H,KHa}$) and potassium ($J_{K,KHa}$) net efflux and the current–voltage relationship (I_{KHa}) of an antiporter that transports n protons for one K^+ ion:

$$J_{H,KHa} = n \cdot \frac{G_{KHa}}{e_0} \cdot ((n-1) \cdot V - n \cdot E_H + E_K) \quad (5)$$

$$J_{K,KHa} = -\frac{G_{KHa}}{e_0} \cdot ((n-1) \cdot V - n \cdot E_H + E_K) \quad (6)$$

$$\begin{aligned} I_{KHa} &= e_0 \cdot (J_{K,KHa} + J_{H,KHa}) \\ &= G_{KHa} \cdot (n-1) \cdot ((n-1) \cdot V - n \cdot E_H + E_K) \end{aligned} \quad (7)$$

with G_{KHa} being the membrane conductance of this transporter type. Analogously to all other transporters, also for the electroneutral 1:1 antiporter ($n = 1$), a parameter G_{KHa0} with the unit of an electrical conductance (pA·mV^{-1}) can be defined, although this transporter does not conduct electrical current. This trick has technical reasons to unify the equations. It is evident for $n = 1$ that $I_{KHa0} = 0$ and that the proportional factor for the fluxes G_{KHA0}/e_0 has the unit mV^{-1}·s^{-1}.

Voltage-gated K^+ channel

Potassium net efflux ($J_{K,KC}$) and the current–voltage relationship (I_{KC}) of a voltage-gated potassium channel:

$$J_{K,KC} = \frac{G_{KC}}{e_0} \cdot p_o(V) \cdot (V - E_K) \quad (8)$$

$$I_{KC} = e_0 \cdot J_{K,KC} = G_{KC} \cdot p_o(V) \cdot (V - E_K) \quad (9)$$

with G_{KC} (pA·mV^{-1}) being the membrane conductance for this channel type. The factor $p_O(V)$ describes the voltage-dependent probability that a channel is open. A suitable mathematical description for hyperpolarization-activated K^+ channels is (Brüggemann et al., 1999) as follows:

$$p_o(V) = \frac{1}{1 + e^{\delta \frac{F}{RT}(V - V_{1/2})}} \quad (10)$$

with $\delta = 1.6$ and $V_{1/2} = -175$ mV. Different values for the gating charge or the half-maximal activation voltage in the physiologically reasonably intervals ($\delta = 0.5 \ldots 2$; $V_{1/2} = -100$ mV $\ldots -200$ mV) did not qualitatively change the results. Actually, the explicit description of the voltage dependence would not be necessary for the steady-state analyses presented in this study (for details see Supplemental Figure S6). For the other channels and transporters, for which less information is available than for K^+ channels, the nonlinearities are implicitly covered by the G_X parameters.

Anion channel

Anion net efflux ($J_{A,AC}$) and the current–voltage relationship (I_{AC}) of an anion channel:

$$J_{A,AC} = -\frac{G_{AC}}{e_0} \cdot (V - E_A) \quad (11)$$

$$I_{AC} = -e_0 \cdot J_{A,AC} = G_{AC} \cdot (V - E_A) \quad (12)$$

with E_A being the Nernst voltage of the anion and G_{AC} (pA·mV^{-1}) the membrane conductance for this channel type.

2 H^+:1 A^- symporter

Proton ($J_{H,HA}$) and anion ($J_{A,HA}$) net efflux and the current–voltage relationship (I_{HA}) of a 2:1 H^+-coupled H^+/A^- symporter:

$$J_{H,HA} = 2 \cdot \frac{G_{HA}}{e_0} \cdot (V - 2 \cdot E_H + E_A) \quad (13)$$

$$J_{A,HA} = \frac{G_{HA}}{e_0} \cdot (V - 2 \cdot E_H + E_A) \quad (14)$$

$$I_{HA} = e_0 \cdot (J_{H,HA} - J_{A,HA}) = G_{HA} \cdot (V - 2 \cdot E_H + E_A) \quad (15)$$

where, G_{HA} is the membrane conductance of this transporter type (pA·mV^{-1}).

Sugar uniporter

Sugar net efflux ($J_{C,SWEET}$) of a sugar uniporter (SWEET type):

$$J_{C,SWEET} = -\frac{G_{SWEET}}{e_0} \cdot E_C \quad (16)$$

with $E_C = \frac{RT}{F} \cdot \ln\left(\frac{[C]_{apo}}{[C]_{cyt}}\right)$ and the apoplastic and cytolic sugar concentrations $[C]_{apo}$ and $[C]_{cyt}$. Although an electroneutral sugar transporter does not have an electrical

conductance, G_{SWEET} and E_C were defined analogously to the other transporters to unify the mathematical description.

Proton-coupled sugar transporter

Proton ($J_{H,HC}$) and sugar ($J_{C,HC}$) net efflux and the current–voltage relationship (I_{HC}) of a 1:1 H^+/C symporter (Carpaneto et al., 2005):

$$J_{H,HC} = \frac{G_{HC}}{e_0} \cdot (V - E_H - E_C) \quad (17)$$

$$J_{C,HC} = \frac{G_{HC}}{e_0} \cdot (V - E_H - E_C) \quad (18)$$

$$I_{HC} = e_0 \cdot J_{H,HC} = G_{HC} \cdot (V - E_H - E_C) \quad (19)$$

with the membrane conductance of this transporter type, G_{HC} (pA·mV^{-1}).

Changes in voltage and concentrations and steady-state conditions

The membrane voltage changes according to the following equation:

$$\frac{dV}{dt} = -\frac{1}{C} \cdot [I_P + I_{KC} + I_{KHs} + I_{KHa} + I_{AC} + I_{HA} + I_{HC} - \Gamma] \quad (20)$$

the cytosolic potassium concentration according to the following equation:

$$\frac{d[K^+]_{cyt}}{dt} = \frac{-1}{Vol \cdot N_A} \cdot [J_{K,KC} + J_{K,KHs} + J_{K,KHa} + J_{K,KHa0} - \Delta K] \quad (21)$$

the cytosolic anion concentration according to the following equation:

$$\frac{d[A^-]_{cyt}}{dt} = \frac{-1}{Vol \cdot N_A} \cdot [J_{A,AC} + J_{A,HA} - \Delta A] \quad (22)$$

and the cytosolic sugar concentration according to the following equation:

$$\frac{d[C]_{cyt}}{dt} = \frac{-1}{Vol \cdot N_A} \cdot [J_{C,SWEET} + J_{C,HC} - C_p + C_c] \quad (23)$$

with the membrane capacitance C, the cellular volume Vol, and the Avogadro constant N_A. The parameters ΔK, ΔA, C_p, and C_c describe concentration changes due to metabolic processes (e.g. photosynthesis, C_p, and respiration, C_c, in the case of sugar) or diffusion into ($\Delta K = \Delta A > 0$) and out of ($\Delta K = \Delta A < 0$) the cell, for example, via plasmodesmata. In special cases, the parameters ΔK, ΔA, and $\Delta C = C_p - C_c$ may also be considered together with $\Gamma = -V \cdot dC/dt$ (Eq. 20 and Supplemental Equation S1) to simulate concentration and voltage changes due to changes in the cellular volume and membrane surface (e.g. guard cell swelling and shrinking). For more details see Supplementary Equations S1 and S2. The steady state analyzed in this study is defined by the following conditions:

$$\frac{dV}{dt} = \frac{d[K^+]_{cyt}}{dt} = \frac{d[A^-]_{cyt}}{dt} = \frac{d[C]_{cyt}}{dt} = 0 \quad (24)$$

Proton concentrations

Proton concentrations are predominantly determined by metabolic processes (Sanders and Slayman, 1982; Wegner and Shabala, 2020; Wegner et al., 2021). Therefore, E_H was fixed to +57.6 mV for the steady-state analyses in this study. This value represented a pH gradient of $pH_{cyt} = 7.0$ and $pH_{apo} = 6.0$ and was chosen without any bias. A different ΔpH, for example, $\Delta pH = 2$ with $E_H = +115.2$ mV, would qualitatively produce the same results.

Renormalization to eliminate a redundant parameter

Equations (20–23) were multiplied by the factor $1 = I_{max}/I_{max}$. I_{max} was combined with the prefactors to I_{max}/C and $I_{max}/(Vol \cdot N_A)$, while $1/I_{max}$ was used to normalize the parameters to the maximal pump current: $i_P(V) = I_P(V)/I_{max}$ (without unit), $g_X = G_X/I_{max}$ (X = KHs, KHa, KHa0, KC, AC, HA, SWEET, HC; all g_X with unit mV^{-1}), $c_p = C_p \cdot e_0/I_{max}$, $c_c = C_c \cdot e_0/I_{max}$, $\Delta c = c_p - c_c$, $\Delta k = \Delta K \cdot e_0/I_{max}$, $\Delta a = \Delta A \cdot e_0/I_{max}$, and $\gamma = \Gamma/I_{max}$ (all without unit). This renormalization eliminated one redundant parameter and yielded the final equation system for the steady-state conditions (Supplementary Equation S3).

Numerical determination of steady-state conditions

For each parameter set g_x the equation system has a steady-state solution for the membrane voltage V and the E_X-values. These were determined first by solving Supplemental Equation S3 and finally by numerically resolving the resultant implicit equations with self-made scripts.

Model assessment

It should be noted that all conclusions drawn in this study are independent of the exact description of the fluxes J_X (Supplemental Figure S6). The screening of the entire reasonable parameter space $[0,\infty)$ for the g_X guaranteed the coverage of all possible cases that a cell can achieve in the considered scenarios, and allowed us to assess the limits of the flexibility of the system under consideration in steady state, even without prior knowledge of specific transporter features.

Supplemental data

The following materials are available in the online version of this article.

Supplemental Equations S1 and S2. Mathematical representation of concentration and voltage changes in swelling or shrinking cells.

Supplemental Equation S3. Mathematical representation of the steady-state conditions of the systems considered in this study.

Supplemental Figure S1. Cases 9 and 10. Combination of anion transporters with the H^+ pump.

Supplemental Figure S2. Cases 12–16. Combination of homeostats with a single transporter for a different ion species.

Supplemental Figure S3. Case 17. Combination of K- and A-homeostats.

Supplemental Figure S4. Consequences of diffusion through plasmodesmata.

Supplemental Figure S5. Consequences of changes in cell size.

Supplemental Figure S6. Equivalence of nonlinear modeling and linear modeling.

Acknowledgments

The author thanks Rob Roelfsema, Würzburg, for helpful discussions regarding membrane potential oscillations in guard cells.

Funding

This research was partially funded by a Fondecyt-Enlace project of the Universidad de Talca.

Conflict of interest statement. None declared.

References

Ahmad I, Maathuis FJM (2014) Cellular and tissue distribution of potassium: physiological relevance, mechanisms and regulation. J Plant Physiol **171**: 708–714

Anschütz U, Becker D, Shabala S (2014) Going beyond nutrition: regulation of potassium homoeostasis as a common denominator of plant adaptive responses to environment. J Plant Physiol **171**: 670–687

Beilby M., Coster HG. (1979) The action potential in Chara corallina III. The Hodgkin-Huxley parameters for the plasmalemma. Funct Plant Biol **6**: 337

Beilby MJ (2007) Action potential in Charophytes. Int Rev Cytol **257**: 43–82

Beilby MJ, Al Khazaaly S (2016) Re-modeling Chara action potential: I. From Thiel model of Ca^{2+} transient to action potential form. AIMS Biophys **3**: 431–449

Beilby MJ, Al Khazaaly S (2017) Re-modeling Chara action potential: II. The action potential form under salinity stress. AIMS Biophys **4**: 298–315

Beilby MJ, Walker NA (1996) Modeling the current-voltage characteristics of Chara membranes: I. The effect of ATP removal and Zero Turgor. J Membr Biol **149**: 89–101

Blatt MR, Beilby MJ, Tester M (1990) Voltage dependence of the Chara proton pump revealed by current-voltage measurement during rapid metabolic blockade with cyanide. J Membr Biol **114**: 205–223

Blatt MR, Wang Y, Leonhardt N, Hills A (2014) Exploring emergent properties in cellular homeostasis using OnGuard to model K^+ and other ion transport in guard cells. J Plant Physiol **171**: 770–778

Böhm J, Scherzer S, Krol E, Kreuzer I, von Meyer K, Lorey C, Mueller TD, Shabala L, Monte I, Solano R, et al. (2016) The venus flytrap *Dionaea muscipula* counts prey-induced action potentials to induce sodium uptake. Curr Biol **26**: 286–295

Britto DT, Kronzucker HJ (2006) Futile cycling at the plasma membrane: a hallmark of low-affinity nutrient transport. Trends Plant Sci **11**: 529–534

Britto DT, Siddiqi MY, Glass ADM, Kronzucker HJ (2001) Futile transmembrane NH_4^+ cycling: a cellular hypothesis to explain ammonium toxicity in plants. Proc Natl Acad Sci USA **98**: 4255–4258

Brüggemann L, Dietrich P, Dreyer I, Hedrich R (1999) Pronounced differences between the native K^+ channels and KAT1 and KST1 alpha-subunit homomers of guard cells. Planta **207**: 370–376

Carpaneto A, Geiger D, Bamberg E, Sauer N, Fromm J, Hedrich R (2005) Phloem-localized, proton-coupled sucrose carrier ZmSUT1 mediates sucrose efflux under the control of the sucrose gradient and the proton motive force. J Biol Chem **280**: 21437–21443

Chen Z-H, Hills A, Bätz U, Amtmann A, Lew VL, Blatt MR (2012) Systems dynamic modeling of the stomatal guard cell predicts emergent behaviors in transport, signaling, and volume control. Plant Physiol **159**: 1235–1251

Chérel I, Gaillard I (2019) The complex fine-tuning of K^+ fluxes in plants in relation to osmotic and ionic abiotic stresses. Int J Mol Sci **20**: 715

Chérel I, Lefoulon C, Boeglin M, Sentenac H (2014) Molecular mechanisms involved in plant adaptation to low K^+ availability. J Exp Bot **65**: 833–848

Choi W-G, Hilleary R, Swanson SJ, Kim S-H, Gilroy S (2016) Rapid, long-distance electrical and calcium signaling in plants. Annu Rev Plant Biol **67**: 287–307

Coskun D, Britto DT, Kronzucker HJ (2010) Regulation and mechanism of potassium release from barley roots: an in planta $^{42}K^+$ analysis. New Phytol **188**: 1028–1038

Coskun D, Britto DT, Li M, Becker A, Kronzucker HJ (2013) Rapid ammonia gas transport accounts for futile transmembrane cycling under NH_3/NH_4^+ toxicity in plant roots. Plant Physiol **163**: 1859–1867

Cuin TA, Dreyer I, Michard E (2018) The role of potassium channels in *Arabidopsis thaliana* long distance electrical signalling: AKT2 modulates tissue excitability while GORK shapes action potentials. Int J Mol Sci **19**: 926

Dindas J, Dreyer I, Huang S, Hedrich R, Roelfsema MRG (2021) A voltage-dependent Ca^{2+}-homeostat operates in the plant vacuolar membrane. New Phytol **230**: 1449–1460

Dreyer I (2017) Plant potassium channels are in general dual affinity uptake systems. AIMS Biophys **4**: 90–106

Dreyer I, Gomez-Porras JL, Riedelsberger J (2017) The potassium battery: a mobile energy source for transport processes in plant vascular tissues. New Phytol **216**: 1049–1053

Dreyer I, Michard E (2020) High- and low-affinity transport in plants from a thermodynamic point of view. Front Plant Sci **10**: 1797

Dreyer I, Spitz O, Kanonenberg K, Montag K, Handrich MR, Ahmad S, Schott-Verdugo S, Navarro-Retamal C, Rubio-Meléndez ME, Gomez-Porras JL, et al. (2019) Nutrient exchange in arbuscular mycorrhizal symbiosis from a thermodynamic point of view. New Phytol **222**: 1043–1053

Dreyer I, Uozumi N (2011) Potassium channels in plant cells. FEBS J **278**: 4293–4303

Farmer EE, Gao Y, Lenzoni G, Wolfender J, Wu Q (2020) Wound- and mechanostimulated electrical signals control hormone responses. New Phytol

Gajdanowicz P, Michard E, Sandmann M, Rocha M, Corrêa LGG, Ramírez-Aguilar SJ, Gomez-Porras JL, González W, Thibaud J-B, van Dongen JT, et al. (2011) Potassium (K^+) gradients serve as a mobile energy source in plant vascular tissues. Proc Natl Acad Sci USA **108**: 864–869

Gilroy S, Trebacz K, Salvador-Recatalà V (2018) Inter-cellular electrical signals in plant adaptation and communication. Front Plant Sci **9**: 643

Gradmann D, Blatt MR, Thiel G (1993) Electrocoupling of ion transporters in plants. J Membr Biol **136**: 327–332

Hedrich R, Salvador-Recatalà V, Dreyer I (2016) Electrical wiring and long-distance plant communication. Trends Plant Sci **21**: 376–387

Hills A, Chen Z-H, Amtmann A, Blatt MR, Lew VL (2012) OnGuard, a computational platform for quantitative kinetic modeling of guard cell physiology. Plant Physiol **159**: 1026–1042

Horaruang W, Hills A, Blatt MR (2020) Communication between the plasma membrane and tonoplast is an emergent property of ion transport. Plant Physiol **182**: 1833–1835

Hosy E, Vavasseur A, Mouline K, Dreyer I, Gaymard F, Porée F, Boucherez J, Lebaudy A, Bouchez D, Véry A-A, et al. (2003) The Arabidopsis outward K+ channel GORK is involved in regulation of stomatal movements and plant transpiration. Proc Natl Acad Sci USA **100**: 5549–5554

Iosip AL, Böhm J, Scherzer S, Al-Rasheid KAS, Dreyer I, Schultz J, Becker D, Kreuzer I, Hedrich R (2020) The Venus flytrap trigger hair-specific potassium channel KDM1 can reestablish the K^+ gradient required for hapto-electric signaling. PLoS Biol **18**: e3000964

Jaślan D, Dreyer I, Lu J, O'Malley R, Dindas J, Marten I, Hedrich R (2019) Voltage-dependent gating of SV channel TPC1 confers vacuole excitability. Nat Commun **10**: 2659

Jezek M, Blatt MR (2017) The membrane transport system of the guard cell and its integration for stomatal dynamics. Plant Physiol **174**: 487–519

Kisnieriene V, Lapeikaite I, Pupkis V, Beilby MJ (2019) Modeling the action potential in Characeae *Nitellopsis obtusa*: effect of saline stress. Front Plant Sci **10**: 82

Luan M, Tang RJ, Tang Y, Tian W, Hou C, Zhao F, Lan W, Luan S (2017) Transport and homeostasis of potassium and phosphate: limiting factors for sustainable crop production. J Exp Bot **68**: 3091–3105

Meckel T, Gall L, Semrau S, Homann U, Thiel G (2007) Guard cells elongate: relationship of volume and surface area during stomatal movement. Biophys J **92**: 1072–1080

Munns R, Day DA, Fricke W, Watt M, Arsova B, Barkla BJ, Bose J, Byrt CS, Chen ZH, Foster KJ, et al. (2020) Energy costs of salt tolerance in crop plants. New Phytol **225**: 1072–1090

Nieves-Cordones M, Alemán F, Martínez V, Rubio F (2014) K^+ uptake in plant roots. The systems involved, their regulation and parallels in other organisms. J Plant Physiol **171**: 688–695

Nizam S, Qiang X, Wawra S, Nostadt R, Getzke F, Schwanke F, Dreyer I, Langen G, Zuccaro A (2019) *Serendipita indica* E5'NT modulates extracellular nucleotide levels in the plant apoplast and affects fungal colonization. EMBO Rep **20**: e47430

Ragel P, Raddatz N, Leidi EO, Quintero FJ, Pardo JM (2019) Regulation of K^+ nutrition in plants. Front Plant Sci **10**: 281

Reyer A, Häßler M, Scherzer S, Huang S, Pedersen JT, Al-Rascheid KAS, Bamberg E, Palmgren M, Dreyer I, Nagel G, et al. (2020) Channelrhodopsin-mediated optogenetics highlights a central role of depolarization-dependent plant proton pumps. Proc Natl Acad Sci USA **117**: 20920–20925

Riedelsberger J, Miller JK, Valdebenito-Maturana B, Piñeros MA, González W, Dreyer I (2021) Plant HKT channels: an updated view on structure, function and gene regulation. Int J Mol Sci **22**: 1892

Riedelsberger J, Vergara-Jaque A, Piñeros M, Dreyer I, González W (2019) An extracellular cation coordination site influences ion conduction of OsHKT2;2. BMC Plant Biol **19**: 316

Rienmüller F, Dreyer I, Schönknecht G, Schulz A, Schumacher K, Nagy R, Martinoia E, Marten I, Hedrich R (2012) Luminal and cytosolic pH feedback on proton pump activity and ATP affinity of V-type ATPase from Arabidopsis. J Biol Chem **287**: 8986–8993

Roelfsema MRG, Steinmeyer R, Staal M, Hedrich R (2001) Single guard cell recordings in intact plants: light-induced hyperpolarization of the plasma membrane. Plant J **26**: 1–13

Sanders D, Slayman CL (1982) Control of intracellular pH: predominant role of oxidative metabolism, not proton transport, in the eukaryotic microorganism neurospora. J Gen Physiol **80**: 377–402

Scherzer S, Federle W, Al-Rasheid KAS, Hedrich R (2019) Venus flytrap trigger hairs are micronewton mechano-sensors that can detect small insect prey. Nat Plants **5**: 670–675

Schott S, Valdebenito B, Bustos D, Gomez-Porras JL, Sharma T, Dreyer I (2016) Cooperation through competition - dynamics and microeconomics of a minimal nutrient trade system in arbuscular mycorrhizal symbiosis. Front Plant Sci **7**: 912

Schwacke R, Schneider A, Van Der Graaff E, Fischer K, Catoni E, Desimone M, Frommer WB, Flügge UI, Kunze R (2003) ARAMEMNON, a novel database for Arabidopsis integral membrane proteins. Plant Physiol **131**: 16–26

Shabala S, Chen G, Chen Z, Pottosin I (2020) The energy cost of the tonoplast futile sodium leak. New Phytol **225**: 1105–1110

Shabala S, Pottosin I (2014) Regulation of potassium transport in plants under hostile conditions: implications for abiotic and biotic stress tolerance. Physiol Plant **151**: 257–279

Sharma T, Dreyer I, Riedelsberger J (2013) The role of K^+ channels in uptake and redistribution of potassium in the model plant *Arabidopsis thaliana*. Front Plant Sci **4**: 224

Sze H, Chanroj S (2018) Plant endomembrane dynamics: studies of K^+/H^+ antiporters provide insights on the effects of pH and ion homeostasis. Plant Physiol **177**: 875–895

Tang R-J, Luan M, Wang C, Lhamo D, Yang Y, Zhao F-G, Lan W-Z, Fu A-G, Luan S (2020) Plant membrane transport research in the post-genomic era. Plant Commun **1**: 100013

Thiel G, MacRobbie EAC, Blatt MR (1992) Membrane transport in stomatal guard cells: the importance of voltage control. J Membr Biol **126**: 1–18

Trebacz K, Dziubinska H, Krol E (2006) Electrical Signals in Long-Distance Communication in Plants. Springer, Berlin, Heidelberg, pp 277–290

Véry A-A, Nieves-Cordones M, Daly M, Khan I, Fizames C, Sentenac H (2014) Molecular biology of K^+ transport across the plant cell membrane: what do we learn from comparison between plant species? J Plant Physiol **171**: 748–769

Vincent TR, Avramova M, Canham J, Higgins P, Bilkey N, Mugford ST, Pitino M, Toyota M, Gilroy S, Miller AJ, et al. (2017) Interplay of plasma membrane and vacuolar ion channels, together with BAK1, elicits rapid cytosolic calcium elevations in Arabidopsis during aphid feeding. Plant Cell **29**: 1460–1479

Ward JM (2001) Identification of novel families of membrane proteins from the model plant *Arabidopsis thaliana*. Bioinformatics **17**: 560–563

Wegner LH, Li X, Zhang J, Yu M, Shabala S, Hao Z (2021) Biochemical and biophysical pH clamp controlling net H^+ efflux across the plasma membrane of plant cells. New Phytol **230**: 408–415

Wegner LH, Shabala S (2020) Biochemical pH clamp: the forgotten resource in membrane bioenergetics. New Phytol **225**: 37–47

Zörb C, Senbayram M, Peiter E (2014) Potassium in agriculture—status and perspectives. J Plant Physiol **171**: 656–669